



**HAL**  
open science

# Seismicity, seismotectonics and crustal velocity structure of the Messina Strait (Italy)

Luciano Scarfi, Horst Langer, Antonio Scaltrito

► **To cite this version:**

Luciano Scarfi, Horst Langer, Antonio Scaltrito. Seismicity, seismotectonics and crustal velocity structure of the Messina Strait (Italy). *Physics of the Earth and Planetary Interiors*, 2009, 177 (1-2), pp.65. 10.1016/j.pepi.2009.07.010 . hal-00585471

**HAL Id: hal-00585471**

**<https://hal.science/hal-00585471>**

Submitted on 13 Apr 2011

**HAL** is a multi-disciplinary open access archive for the deposit and dissemination of scientific research documents, whether they are published or not. The documents may come from teaching and research institutions in France or abroad, or from public or private research centers.

L'archive ouverte pluridisciplinaire **HAL**, est destinée au dépôt et à la diffusion de documents scientifiques de niveau recherche, publiés ou non, émanant des établissements d'enseignement et de recherche français ou étrangers, des laboratoires publics ou privés.

## Accepted Manuscript

Title: Seismicity, seismotectonics and crustal velocity structure of the Messina Strait (Italy)

Authors: Luciano Scarfì, Horst Langer, Antonio Scaltrito

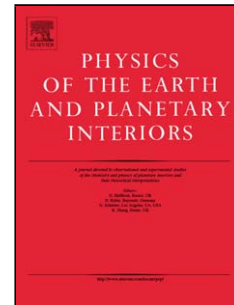
PII: S0031-9201(09)00154-X  
DOI: doi:10.1016/j.pepi.2009.07.010  
Reference: PEPI 5186

To appear in: *Physics of the Earth and Planetary Interiors*

Received date: 11-11-2008  
Revised date: 24-6-2009  
Accepted date: 9-7-2009

Please cite this article as: Scarfì, L., Langer, H., Scaltrito, A., Seismicity, seismotectonics and crustal velocity structure of the Messina Strait (Italy), *Physics of the Earth and Planetary Interiors* (2008), doi:10.1016/j.pepi.2009.07.010

This is a PDF file of an unedited manuscript that has been accepted for publication. As a service to our customers we are providing this early version of the manuscript. The manuscript will undergo copyediting, typesetting, and review of the resulting proof before it is published in its final form. Please note that during the production process errors may be discovered which could affect the content, and all legal disclaimers that apply to the journal pertain.



## 1                    **Seismicity, seismotectonics and crustal velocity structure of the Messina Strait (Italy)**

2                    Luciano Scarfi, Horst Langer, and Antonio Scaltrito

3                    *Istituto Nazionale di Geofisica e Vulcanologia, sezione di Catania, Piazza Roma, 2, 95123 Catania, Italy*

### 4

### 5   **Abstract**

6   The Messina Strait is the most important structural element interrupting the southernmost part of the Alpine-Apenninic  
7   orogenic belt, known as the Calabro-Peloritan Arc. It is being a narrow fan-shaped basin linking the Ionian Sea to the  
8   Tyrrhenian Sea. This region is affected by considerable seismic activity which mirrors the geodynamic processes due to  
9   the convergence between the African and the Eurasian plates. In the last four centuries, a significant number of  
10   disastrous earthquakes originated along the Arc. Among these, the most noteworthy event occurred on December 28,  
11   1908 (known as the Reggio Calabria-Messina earthquake), in the Messina Strait area and caused a large tsunami and  
12   more than 100,000 casualties. In this research we focus on the relationships between the general tectonic setting, which  
13   characterize the Messina Strait and adjacent areas, seismicity patterns and the crustal structure. We analyzed a data set  
14   consisting of more than 300 events occurring in the years from 1999 to 2007, having a magnitude range from 1.0 to 3.8.  
15   This data set was exploited in a local earthquake tomography, by carrying out a simultaneous inversion of both the  
16   three-dimensional velocity structure and the distribution of seismic foci. We applied the “tomoADD” algorithm, which  
17   uses a combination of absolute and differential arrival times and a concept of self-adapting grid geometry, accounting  
18   for ray density encountered across the volume. With this method the accuracy of event locations is improved and  
19   velocity structure near the source region is resolved in more detail than standard tomography.

20   Fault plane solutions were obtained for the major and best-recorded earthquakes. The obtained velocity images  
21   highlight vertical and lateral heterogeneities that can be associated with structural features striking from NNE-SSW to  
22   NE-SW. These results are consistent with important tectonic elements visible at the surface and the pattern delineated  
23   by earthquake locations and focal mechanisms.

24

25   *Keywords:* Crustal structure, Focal mechanism, Seismicity, Seismotectonics, Tomography

## 28 1. Introduction

29

30 A hundred years have now passed since the disastrous earthquake on December 28, 1908, one of the largest events ever  
31 recorded in the central Mediterranean (Boschi et al., 2000), destroyed Messina, Reggio Calabria and the adjacent areas.

32 In addition to the damage due to the impact of the seismic waves, much destruction and loss of life was caused by a  
33 tsunami which developed as a consequence of the earthquake.

34 The Messina Strait is without doubt the most important structural element interrupting the southernmost part of the  
35 Alpine-Apenninic orogenic belt, known as the Calabro-Peloritan Arc. (Fig. 1). It forms a branch of the Ionian Sea  
36 separating SW Calabria from NE Sicily. Its western margin belongs to an escarpment that stretches over 70 km from  
37 Messina towards the Mt. Etna area. In W - E direction, the elevation falls from about 1000 a.s.l. to a depth of more than  
38 1000 b.s.l. in the center of the Strait, which means a total elevation difference of 2000 m along a distance of less than 20  
39 km. The considerable orographical differences in NE Sicily, SW Calabria and in the Ionian Sea are the expression of  
40 intense tectonic activity. Indeed, from a seismotectonic point of view, the Calabro-Peloritan Arc region is characterized  
41 by considerable geodynamic instability (Gasparini et al, 1982; Monaco and Tortorici, 2000; CPTI work group, 2004). In  
42 the last four centuries, a considerable number of violent earthquakes, with epicentral intensities of 10 to 11 degrees  
43 MCS (CFTI-Med 4.0), have occurred along the sector of the Arc stretching from the Gulf of S. Eufemia to the Nebrodi  
44 Mountains. A significant aspect of this activity is the devastating impact produced on the ground: massive landslides  
45 that narrow and sometimes obstruct valleys, the formation of small lakes, the deviation of watercourses, slumps, and the  
46 fracturing and liquefaction of soil (Bottari et al., 1986; Murphy, 1995; Galli, 2000; Tertulliani and Cucci, 2008). These  
47 dramatic phenomena of ground failure are generally considered indicative of the shallow depth of the earthquake  
48 source. Indeed, analyses of the macro-seismic fields of the best-documented events favor the hypothesis of a position of  
49 the sources – or part of them - close to the surface (see, e.g. Bottari et al, 1986). However, the lack of surface faulting  
50 after the largest shocks makes the understanding of the source location as well as the geometry of the fault system a  
51 difficult task. We have no ground proof as to whether the important topographical elements around the Messina Strait  
52 form true fault systems, perhaps cutting the entire crust and reaching the upper mantle. The identification of such fault  
53 systems is further hindered by the great depth of the Ionian Sea (more than 1000 m in the southern part of the Messina  
54 Strait) - clearly, there are difficulties in recognising geological formations and tectonic structures underlying the  
55 juvenile sediments covering the sea floor at such depths. As a consequence, the dislocation nature of the 1908 Messina  
56 Strait earthquake has been a matter of debate (see web site of DISS). Ghisetti (1984) has suggested a graben-like style  
57 of faulting for the Messina Strait. For other authors (e.g. Valensise and Pantosti, 1992), the fault causing the 1908

58 Messina Strait earthquake is seen as a low angle, blindly ending element dipping east, rather than a steeply westward  
59 dipping structure parallel to the northeastern coast of Sicily (e.g. Bottari et al., 1986).

60 Research efforts by various institutions have enabled collecting a sizeable set of seismic records, disclosing the  
61 possibility of an in-depth investigation of seismotectonic patterns in the area. In particular, the Istituto Nazionale di  
62 Geofisica e Vulcanologia has been running a permanent local seismic network from 2001 on; before this time the  
63 network was operated by the “Sistema POSEIDON” since the middle of the 1990’s. In a recent paper, Barberi et al.  
64 (2004) investigated the 3D velocity structure on a fairly wide scale (40 km horizontal grid spacing and 10 km in vertical  
65 direction) in an area covering the Southern Tyrrhenian Sea and the Calabrian Arc region. In this investigation, a positive  
66 velocity anomaly was found in the Messina Strait at a depth of about 15 km. A further feature of interest here is a  
67 negative anomaly stretching from the area north of Mt Etna in ENE direction into the Ionian Sea and the southern tip of  
68 the Italian peninsula.

69 In this research, we focus on the relationship between the general tectonic setting, which characterizes the Messina  
70 Strait and adjacent areas, seismicity patterns and the crustal structure. We used a data set consisting of a total of 360  
71 events with a magnitude range from 1.0 to 3.8 occurring in the period from 1999 to 2007. This data set is exploited in a  
72 local earthquake tomography (LET), by carrying out a simultaneous inversion of both the three-dimensional velocity  
73 structure and the distribution of seismic foci.

74 In conventional LET (e.g. using the SimulPS12 code; see Evans et al., 1994) the inversion of velocity parameters and  
75 earthquake location is carried out on the basis of absolute arrival time readings. These locations are affected by errors  
76 collected over the whole ray path, hence the risk that velocity perturbations outside the well illuminated area are  
77 mapped into it. Furthermore, the use of absolute arrival times typically requires the definition of station corrections in  
78 order to minimize site effects. One way round this dilemma is to use differential travel times, as proposed for instance  
79 by Waldhauser and Ellsworth (2000). For earthquake clusters, with foci lying close to each other, travel time errors due  
80 to incorrect velocity models in the volume outside the cluster will essentially cancel out. As a consequence of using  
81 relative travel times, the use of station corrections becomes obsolete. At the same time, it can be shown (see e.g.  
82 Waldhauser and Ellsworth, 2000; Menke and Schaff, 2004) that the use of differential travel times considerably  
83 improves the relative locations and provides at least the same quality of absolute hypocenter locations as do standard  
84 location techniques. Conventional LET uses a velocity grid defined in Cartesian coordinates and with a regular cell or  
85 grid spacing to be defined a priori. The advantage of working with fixed cells lies in its simplicity. For instance, such  
86 velocity grids can easily be used in Monte Carlo experiments (see Raffaele et al., 2006) in order to examine the  
87 statistical stability of the results. However, the ray distribution is typically highly uneven due to non-uniform station  
88 configuration, the distribution of hypocenters and ray bending. The regular grid geometry makes it difficult to adapt to

89 the unevenness of the rays with the outcome that some cells may have few or no rays, while others may have a very  
90 high ray density sampling. Ideally, the inversion grid should be distributed adaptively to match the resolving power of  
91 the data (see Zhang and Thurber, 2005).

92 Zhang and Thurber (2003, 2005) developed computer codes which allow to bypass the problems encountered with  
93 absolute hypocenter locations and inflexible velocity grids. Here, we have been using their code tomoADD. Both  
94 absolute and relative arrival time readings can be used. The accuracy of the latter can be improved for multiplet events,  
95 where relative arrival times can be obtained using correlation and coherency based techniques, such as the cross-  
96 spectral method. In the adaptive generation of the velocity grid, new grid points are inserted in a tetrahedron of former  
97 grid points if a certain threshold value of weighted ray density (DWS) is reached. At the same time, older grid points  
98 may be removed if their DWS falls below a limiting value. For more details, see Zhang and Thurber (2005).

99 Finally, our preference for TomoADD was justified from a comparison of the overall RMS travel time residuals  
100 obtained with the classical LET method (Evans et al., 1994). TomoADD gave considerably lower residuals (0.13 s) than  
101 classical LET using the SimulPS12 code, where an overall residual of 0.29 s was encountered.

102

## 103 **2. Tectonic Setting**

104

105 The investigated area belongs to the Calabro-Peloritan Arc, which is part of the Apennine-Maghrebian orogenic belt  
106 along the Africa-Europe plate boundary. In this sector, convergence processes, from the Neogene-Quaternary on, led to  
107 the formation of three distinct tectonic domains: i) the Tyrrhenian back-arc basin (extensional domain), ii) the Alpine-  
108 Apenninic orogenic belt (domain of crust shortening) and iii) the Hyblean Foreland (Fig. 1). The Calabro-Peloritan Arc  
109 connects the NW-SE-trending southern Apennines with the WSW-striking Maghrebian thrust zones (Fig. 1). Its recent  
110 geodynamic evolution has been closely related to the opening of the Tyrrhenian Sea beginning in the middle Miocene,  
111 the ESE-ward drift of the Calabro-Peloritan massif and the subduction of Ionian oceanic lithosphere underneath  
112 Calabria (Finetti and Del Ben, 1986). Several, often contrasting hypotheses, have been proposed for the current  
113 geodynamic of the area, such as active subduction beneath the southern Tyrrhenian Sea (Barberi et al., 1973), or rifting  
114 dominated by slab sinking and passive subduction (Finetti and Del Ben, 1986; Patacca et al., 1990). Debate on the most  
115 appropriate model is still open. However, the presence of a subducted slab is marked by the occurrence of intermediate  
116 and deep earthquakes (between 50 and 400 km) beneath the southern Tyrrhenian Sea, along a NW-dipping Benioff zone  
117 (Gasparini et al., 1982; Anderson and Jackson, 1987; Giardini and Velonà, 1991), and by a seismic high-velocity  
118 anomaly in the mantle (e.g. Selvaggi and Chiarabba, 1995).

119 The Messina Strait is the most important structural discontinuity cutting the southern part of the Arc, forming a narrow  
120 fan-shaped basin linking the Ionian Sea to the Tyrrhenian Sea. Following Ghisetti (1992), it is bounded by high angle  
121 normal faults with prevailing N-S to NE-SW orientation, and identified as active during Pliocene and Pleistocene times.  
122 Among the major faults, the Larderia-Curcuraci fault system bounds the eastern margin of Sicily. The Reggio Calabria-  
123 Calanna-S. Eufemia and the Armo-Delianuova fault systems are situated on the Calabrian side of the Strait. Other NW-  
124 SE and E-W striking fault families contribute to a rather complex structural picture, particularly in Calabria (Fig. 1).  
125 Consequently, long-term evolution and the structural setting of the Strait are still a matter of discussion (see among  
126 others: Valensise and Pantosti, 1992; Tortorici et al., 1995).

127 Seismological, geodetic and structural data demonstrate that the studied area is characterized by active extensional  
128 tectonics, at least in the upper part of the crust between depth from surface to 15 km. Indeed, several authors (Tortorici  
129 et al., 1995; D'Agostino e Selvaggi, 2004; Neri et al., 2004) claim two different styles of deformation accommodating  
130 the Europa-Africa convergence in Sicily and in the Calabro-Peloritan Arc. In their opinion the area to the west of the  
131 Aeolian-Tindari-Giardini lineament (ATG) is dominated by a compressional regime presumably induced by plates  
132 convergence. The area to the east of the lineament is characterized by NW-SE extension that may be related to an  
133 Ionian subduction slab rollback.

134

### 135 **3. Data Set and Seismicity**

136

137 We analyzed seismicity in the area of the Messina Strait by using the data recorded the local network operated by the  
138 "Sistema POSEIDON" and subsequently by Istituto Nazionale di Geofisica e Vulcanologia in eastern Sicily and  
139 southern Calabria since the 1990's (Fig. 1b). The network consists of three-component stations. Since 2004, stations  
140 with analogical telemetry have been upgraded with modern digital VSAT based data transmission and equipped with  
141 three-component broadband sensors (40 s). In order to reduce the azimuth gap, the stations of the nearby Aeolian  
142 Islands, Mt. Etna and of the National permanent seismic networks are occasionally included as they provide additional  
143 onset readings for the most energetic events. All the stations use the same base time, set by GPS time.

144 In the area extending from  $37.81^{\circ}$  N to  $38.33^{\circ}$  N, and  $15.35^{\circ}$  E to  $16.01^{\circ}$  E, about 360 earthquakes (Fig. 2) were  
145 recorded between 1999 and 2007. In the hypocenter distribution, with coordinates taken from INGV-CT catalogue (see  
146 <http://www.ct.ingv.it/Sismologia/analisti/default.asp>), we recognize a concentration of foci within the uppermost 15-20  
147 km. A similar limitation of focal depth in the Peloritani Mountains has been explained by Langer et al. (2007) in terms  
148 of a "Brace-Goetze Lithosphere", where rock rheology is assumed to depend on depth and temperature (for more details  
149 on this subject see also Stüwe, 2002). Greater depth encountered in the south may be related to the presence of the

150 subducted slab, but this must be read with caution as location uncertainties increase due to the unfavorable network  
151 configuration. Most of the earthquakes are located within three zones: i) in southwestern Calabria (inland), ii) in the  
152 Strait between Messina and Reggio Calabria and iii) in the Ionian Sea, west of Cape S. Alessio. On the other hand, very  
153 few events were located in the inland area, between Cape S. Alessio and the northeastern tip of Sicily.

154 For our investigation, we filtered the original data set according to quality criteria of location. In particular, we selected  
155 only well located events, i. e. those with at least 9 observations (P- and S-phases), root-mean-square (RMS) residuals  
156 smaller than 0.35 s and horizontal and vertical location errors lower than 2.5 km and 3.5 km, respectively. We also  
157 tested the location stability - using the tomoADD code but keeping the velocity parameters fixed - by shifting the trial  
158 hypocenters randomly in the space (see Husen et al., 1999). This helped identify events for which different locations  
159 with equivalent travel-time residuals can be found. Note that the presence of events with unstable locations bears the  
160 risk of introducing biases as the inversion process may decrease the travel-time residuals by shifting around the  
161 hypocenter coordinates instead of adjusting the velocity model parameters properly. In practice, we have compared the  
162 locations with unperturbed starting solutions and the locations with starting solutions to which a random perturbation of  
163 up to  $\pm 8$  km was added. We repeated the test five times and considered the realisations where the difference between  
164 the solutions were maximum. In doing so, we have a conservative estimate of the stability of the hypocenter locations  
165 by removing events with horizontal or vertical location variations greater than 3 km. All tests revealed fairly stable  
166 epicenter determinations for almost all the events. In fact, the differences of the results with non-perturbed starting  
167 locations and results with randomly perturbed ones was fairly low (1 km or less for 96% of the well locatable events  
168 matching the quality criteria mentioned above). Finally, we obtained a data set of 244 well locatable and stable events  
169 which were used in the simultaneous inversion of both the velocity structure and the hypocenter location.

170

#### 171 **4. 3D Imaging**

172

173 A total of 1785 P and 1163 S absolute arrival times and about 46250 catalogue-derived differential times were jointly  
174 inverted using the tomoADD algorithm (Zhang and Thurber, 2005) for hypocentral parameters and velocity structure.

175 For the given amount of S-wave data available, however, we limit ourselves to discuss the velocity model for P-waves  
176 and address to further studies with an enriched data set, when in particular more S-wave arrival times will be available.

177 We decided to reduce the weight of S-wave arrivals to 20% for fitting the velocity model, whereas their full weight is  
178 maintained for the hypocenter location. In doing so, we avoid that S-wave velocities, which are less constrained than  
179 those for P-waves, are shifted around artificially reducing the overall residuals.



180 We started the inversion from a regular horizontal grid, with 5x5 km node spacing covering an area of 60x60 km, based  
181 on the P and S ray paths of the selected data obtained by the pseudo-bending method (Um and Thurber, 1987) (Fig. 3).  
182 Vertical grid spacing varies between 2 and 6 km and covers a depth range from the surface to 33 km depth, following  
183 the 1D reference velocity model (Langer et al., 2007). Higher weighting was applied first to the catalogue absolute data  
184 in order to obtain a large-scale result. Then, higher weights were assigned to the differential data to refine the event  
185 locations and the velocity structure near the source region. The damping values were selected on the basis of L-  
186 curves of solution and data variances (see Zhang and Thurber, 2005).

187 The number and position of inversion mesh nodes change from one iteration to the next as the method automatically  
188 adjusts the inversion mesh nodes according to the data distribution. The procedure implemented in TomoADD is based  
189 on the construction of tetrahedral and Voronoi diagrams and the use of the Qhull algorithm (see Zhang and Thurber,  
190 2005). In this way, the density of the inversion mesh nodes is higher in volumes where more rays are passing. The  
191 strategy applied in tomoADD for the design of the mesh is based on the derivative weight sum (DWS), which quantifies  
192 the ray density around each model node. DWS is a key parameter for understanding how well the model is resolved  
193 (Haslinger et al., 1999). Moreover, the adaptive mesh method considers the different ray distribution between the P and  
194 S waves. At the end of the iterative process, the inversion mesh nodes for P and S waves are irregularly distributed,  
195 accounting for the heterogeneous distribution of the rays (Fig. 4). As a result, ray sampling for each inversion mesh  
196 node is more uniform and the tomographic system proves more stable than in a conventional grid with regular spacing  
197 (e.g. Zhang and Thurber, 2005).

198 In Fig. 5, we compare the distribution of the DWS for a conventional regular mesh created with tomoDD and the one  
199 obtained with tomoADD. In the latter, we notice 1379 nodes with non-zero DWS values, all having DWS values greater  
200 than 100. The average DWS value is 390 with standard deviation 133. With regular inversion grid (tomoDD), there are  
201 1359 nodes with non-zero DWS value, among which only 36% of them have DWS values greater than 100. Many  
202 inversion grid nodes have DWS values less than 10 and the average DWS value is 286. In other words, the adaptive  
203 strategy of mesh creation in tomoADD exploits the available information efficiently, whereas the regular grid yields a  
204 highly uneven DWS distribution, which becomes a critical issue when only a limited amount of data is available.

205 Fig. 6 shows the three dimensional velocity structure for P-wave velocities in the Messina Strait area. We have marked  
206 the zones with a reasonable illumination ( $DWS > 100$ ) with a yellow line. The shallowest layers, at a depth of 6 and 8  
207 km, are characterized by strong positive anomalies in the northern part of the Messina Strait, as well as in the area of the  
208 Mts Peloritani and the Mt. Aspromonte. Positive P-wave anomalies are also found more southward along the eastern  
209 coast of Sicily, in particular in the offshore area of the Cape S. Alessio. A negative anomaly occurs on the Calabrian  
210 side, in an area lying more or less between the Reggio Calabria-Calanna-S. Eufermia and the Armo-Delianuova fault

211 systems. A similar picture is found at a depth of 10 km, with higher P-wave velocities from north, in the Strait,  
212 southward, along the eastern coast of Sicily, interrupted by lower velocity zones with trends cutting the coastline.  
213 Again, we notice relatively high P-velocities in the Mts Peloritani and in the Mt. Aspromonte. A negative anomaly is  
214 clearly visible in a northeast-southwest striking stripe from the southern part of the Strait to the fault systems of the  
215 Calabrian side. At deeper layers (12 and 15 km depth) we notice a slightly modified picture. In fact, in the central and  
216 southern parts of the studied area, we notice two zones of low P-wave velocities, trending about ENE-WSW, separated  
217 by a ridge with high P-wave velocities. At a depth of 18 km the aforementioned structures are still identifiable, though  
218 the picture is blurred by the worsening illumination at this depth. Cross-sections of  $V_p$  are displayed in Fig. 7.

219

## 220 **5. Stability Analysis with Monte Carlo Tests**

221

222 Monte-Carlo tests are popular instruments in parameter studies, used to check the stability of forward and inverse  
223 modeling. They have the advantage of making very limited a-priori assumptions about possible errors. However, they  
224 entail an additional computational burden as the inversions have to be repeated a number of times. This additional effort  
225 becomes affordable with increasing computer capacities. During the Monte Carlo tests, we have added uniformly  
226 distributed random disturbances to our input data, i.e. the arrival times and the starting velocity model. In particular,  
227 uncertainties of the arrival time readings were accounted for by adding a random perturbation of up to  $\pm 50$  ms for first  
228 onset readings and up to  $\pm 100$  ms for S-phase arrival times. The starting velocity model has been examined in detail by  
229 Langer et al. (2007) and was found to be the best available one. Nonetheless, as its parameters make up part of the input  
230 information we examined the effect of possible uncertainties. We applied random perturbations in the range of  $\pm 0.1$   
231 km/s both for the P- and S-wave velocities. We repeated the Monte Carlo test 15 times in order to achieve a reasonable  
232 significance. Focusing on grid nodes with DWS of at least 100, we found 50 percent of all nodes (i. e. nodes between  
233 the 25 % and 75% quartiles) scatter in the range of  $\pm 110$  m/s around the results without random perturbation. The  
234 standard deviations for the velocity models give a range of  $\pm 130$  m/s.

235 The travel time residuals are the measure of the goodness of fit for the inverted model. A comparison of residuals  
236 obtained with and without randomization helps understand whether the assumed uncertainties of input data are realistic  
237 or overestimated. In the first case, we expect that travel time residuals obtained with randomization are equivalent to  
238 those without, as the accuracy of input data is essentially unaltered. In the second case, we expect that the quality of  
239 inverted models worsens significantly. In our case, all inversions carried out with perturbed input data gave slightly  
240 higher travel time residuals (about 10% for both absolute and weighted) than the inversion carried out without  
241 randomization. We thus conclude that the assumed uncertainties, with respect to arrival time readings and initial guess

242 of the velocity model, are on the safe side as the random perturbation applied to the input data tends to overestimate the  
243 true inaccuracy of input parameters. This implies that the expected scatter of the inverted velocity parameters, as far as  
244 being caused by the uncertainty of the input parameters, also represents a conservative estimate. On the other hand, we  
245 may consider these values a measure of lower threshold for distinguishable anomalies. Velocity differences in the  
246 tomographic image which are of the order of 100 to 130 m/s might merely be an effect of an uncertainty of arrival time  
247 picking or the parameters of the initial velocity model.

248

## 249 **6. Synthetic Testing**

250

251 Overall, travel time residuals, DWS and other parameters furnish first-order diagnostics for the assessment of the  
252 resolution, whose real significance depends on the individual conditions of the inversion problem and whose  
253 understanding needs intuition. We therefore carried out numerical experiments with synthetic models, which give an  
254 immediate and straightforward idea of the inversion stability, potentially insignificant or artificial features and the  
255 sensitivity with respect to the choice of the starting model. Here, we have used synthetic travel times calculated for  
256 typical test models. These data were then inverted using the same starting model, choice of parameters and control  
257 values as for the real data.

258 One type of synthetic test to assess the structural resolving power is the restoring resolution test (Zhao et al., 1992). It  
259 consists of calculating the synthetic travel times for both the velocity model and hypocenter locations obtained through  
260 the inversion. Additionally, noise is added to both travel times and initial guesses. By comparing the results of the  
261 inversion of synthetic travel times with those obtained with the real data, we can estimate the restoring capacity of the  
262 data set. A major problem of such a restoring resolution test may be local minima in areas of low resolution, leading to  
263 the impression of good resolution in actually unresolved areas. The use of a characteristic model avoids this difficulty  
264 (Haslinger et al., 1999). A characteristic model contains the size and the amplitude of anomalies seen in the inversion  
265 results, but with different sign of the amplitude. It is highly unlikely that such a model will represent the same  
266 mathematical minimum as the one obtained with the real data. Therefore, areas of low resolution will be indicated by  
267 not restoring the characteristic model.

268 We performed both synthetic tests. Following the strategy of the characteristic model (see Haslinger et al., 1999), we  
269 designed a velocity model with anomalies at the same position as the ones encountered from the original model but of  
270 opposite sign; i. e. positive anomalies become negative, negative become positive. The absolute deviations are  
271 maintained. As in our original inversion we started with the optimum 1D model proposed by Langer et al. (2007) and  
272 applied TomoADD to the synthetic travel times. In the characteristic test we noted that the position and sign of the

273 velocity anomalies are recovered fairly well, at least for nodes where DWS was higher than 100. However, the amount  
274 of anomalies is considerably smaller, with a model variance underestimating the true one (Fig. 8a). Travel time  
275 residuals for the inverted test model were about 30 ms.

276 With the restoration test we followed a similar strategy to that applied by Scarfi et al (2007). We calculated synthetic  
277 travel times for the inverted velocity structure and hypocenter locations. Subsequently, we applied a random  
278 perturbation to travel time. Carrying out the inversion without applying random perturbation to the input parameters we  
279 achieved a similar travel time residual as with the characteristic model, i. e. 30 ms. Again, the inverted anomalies are  
280 similar to the a-priori ones, with respect to position and sign (Fig. 8b). On the other hand, their amount was found  
281 smaller than the a-priori values, leading to smaller model variance. With noisy input parameters (perturbations taken  
282 from the Monte Carlo experiments, with up to  $\pm 50$  ms for P-wave onsets,  $\pm 100$  ms for S-phase picking) the travel time  
283 residuals increase to about 50 ms. The residuals reach 100 ms, when an additional systematic error of up to 0.2,  
284 representing for instance station corrections, is assumed. The overall characteristic of results is the same as before, in  
285 the sense that inverted and a-priori anomalies match both with respect to their position and sign, whereas the inverted  
286 model tends to be considerably smoother than the a-priori one.

287

### 288 7. 3D Location

289

290 Besides the velocity model, seismic tomography also introduces modifications of the hypocenter location. Compared to  
291 the original locations our revised ones show a major degree of clustering (e.g. see the clusters marked with S1 and S2 in  
292 Fig. 9). This is no surprise since tomoADD – similar to HypoDD - is based on travel time differences between the  
293 events and a major clustering of hypocenters has already been noted in the literature when travel time differences  
294 between event clusters are used instead of single absolute arrival time readings (see, e.g. Waldhauser and Ellsworth,  
295 2000; Scarfi et al., 2005). In our final locations obtained with tomoADD (Fig. 9), we recognize epicenters nicely  
296 aligned along the Reggio Calabria-Calanna-S. Eufemia and the Armo-Delianuova fault systems. A further linear  
297 alignment of epicenters, striking in a NW direction is found offshore Cape Taormina.

298 The clusters of events marked as S1 and S2 form two families of multiplet events with very similar waveforms, which  
299 can be exploited for high precision relative location analysis. We examined the geometry of the two families in more  
300 detail using high precision relative location with the master-event technique (e.g. Scarfi et al., 2005) and performed a  
301 Principal Component Analysis (PCA) on the covariance matrix of the relative hypocenter locations (see Figs. 10a and  
302 10b). For S2, taking the eigenvalues and corresponding eigenvectors, we infer a cluster forming a N 30° E striking  
303 planar element with a dip of 70° W. From the square root of the largest eigenvalue and its eigenvector we obtain a

304 hypocenter cloud elongated about 1100 m (68% value, in terms of confidence given by  $\pm$  one standard deviation) in a  
305 more or less horizontal direction. Using the same technique, for the S1 cluster, we found a major elongation in a N 20°  
306 W striking direction and a dip of about 80° E. We estimate an extension of the data cloud corresponding to about 360  
307 m. In both S1 and S2 clusters, the smallest extension, measured perpendicular the plane spanned by the two major  
308 eigenvectors, is of the order of 140 m. This is close to the possible uncertainty of relative location due to intrinsic  
309 inaccuracy of travel time determination (see Scarfi et al., 2005).

310

## 311 **8. Fault Plane Solutions and Tectonic Structures.**

312

313 Fault plane solutions were obtained for the major and best recorded earthquakes occurring in the years 1999-2007. The  
314 solutions are based on first arrival P-wave polarities. The nodal lines were identified using the code published by  
315 Reasenberg and Oppenheimer (1985). On the basis of the fault plane solutions and considering patterns inferred from  
316 event locations, we may distinguish four seismotectonic regimes: (i) the Messina Strait, (ii) the Mt. Aspromonte, (iii)  
317 the Ionian Sea adjacent to the southernmost coast of Calabria, (iv) the offshore region of Cape Taormina and Cape S.  
318 Alessio (see Fig. 11).

319 The Messina Strait area is characterized by normal faulting events along NE to NNE striking planes, with almost  
320 vertical P-axes, and T-axes striking WNW-ESE. Similar patterns were reported by Scarfi et al. (2005) and Giammanco  
321 et al. (2008) for the nearby Peloritani Mountains area in northeastern Sicily (see also Fig. 11). The orientation of the  
322 nodal planes is also consistent with the orientation of the S2 cluster as well as the earlier mentioned epicenter  
323 alignments in Calabria. In the Mt. Aspromonte normal faulting as well as strike slip solutions were found, with vertical  
324 P-axes or horizontal P-axes striking NNE. In the figure, it can be seen that nodal planes follow trends of tectonic  
325 structures visible at the surface. In the Ionian Sea close to the southernmost coast of Calabria the earthquakes show a  
326 prevailing normal faulting mechanism with a minor strike slip component, and an extension in NE direction. In the  
327 offshore area of Cape Taormina and Cape S. Alessio, there are two events with clear strike slip movement and two  
328 normal faults with T-axes oriented WNW-ESE.

329

## 330 **9. Discussion and conclusions**

331

332 In this paper we have investigated the three dimensional velocity structure in the Messina Strait area. In this context, we  
333 re-evaluated the seismicity patterns by relating them to fault plane solutions and tectonic evidences visible at the  
334 surface. Seismic tomography was carried out using the recently developed code tomoADD (Zhang and Thurber, 2005),

335 which gave the best arrival time residuals compared to the more classical codes SimulPS12. TomoADD uses absolute  
336 arrival times as well arrival time differences among earthquake clusters, and applies a flexible concept of mesh  
337 generation. Compared to conventional local earthquake tomography, tomoADD gives at least the same accuracy of  
338 earthquake location and guarantees a more homogeneous illumination of the grid cells. The inversion thus makes a  
339 more efficient use of the available data set and improves the reliability of results.

340 We have assessed the stability of our inverted model with respect to uncertainties of the input parameters by applying a  
341 Monte Carlo test. We also analyzed the resolution capabilities of the data set, in particular using the DWS distribution  
342 and performing synthetic tests. We found that the velocity structure is well resolved at least for nodes where DWS was  
343 equal/higher than 100. This condition is met in layers with depth ranging from 6 km to 18 km. From synthetic tests we  
344 infer, that the position and sign of velocity anomalies can be recovered fairly well, however, underestimating the  
345 variance of the velocity model. In this light our results are understood as a smooth, i. e., conservative estimate of the  
346 true heterogeneity of the structure of the crust.

347 A major point for discussion concerns the structural setting of the Messina Straits and thus the geometry of the  
348 seismogenic faults. From the pattern of high- and low-velocity anomalies visible in the layers at different depths as well  
349 as in the cross-sections (Figs 6 and 7), we identify a NE-SW striking stripe with negative velocity anomalies. On the  
350 Calabrian mainland, this stripe essentially coincides with the zone delimited by the Reggio Calabria – Calanna - S  
351 Eufemia (northern border) and Armo - Delianuova faults (southern border, see Fig. 7, cross-sections A-A'', B-B'', C-C''  
352 and also F-F''). The continuation of this trend in the Ionian Sea can be readily identified in the southernmost profiles,  
353 closer to the NE-Sicily coast. Clear positive P-wave velocity anomalies are found in the northern part of the Messina  
354 Strait and along the eastern coast of Sicily. The positive anomaly in the Peloritani Mountains is separated from the one  
355 of the Strait by a narrow but evident stripe of relatively low velocities. In the deeper layers (12, 15 and 18 km) we  
356 notice a ridge of positive anomalies starting in the area of Cape Taormina, then bending in an ENE direction. The ridge  
357 crosses the Ionian Sea and is also found in Calabria. For the sake of clarity, figure 12 shows the topography of the 6.5  
358 km/s  $V_p$  isosurface which summarizes the main features of the obtained velocity structure. In the figure, we also plot the  
359 epicenter of the earthquakes located above the isosurface.

360 Our locations were carried out for a revised data set, focusing on earthquakes satisfying specific quality criteria with  
361 respect to the number of available arrival time readings, stability of the starting solution for the hypocenter location, and  
362 the goodness of fit (residual). The critical selection of events is necessary in order not to bias the inversion, but also to  
363 avoid artifacts, which could be erroneously interpreted as seismotectonic patterns (see Scarfi et al., 2003, 2005).

364 Seismic foci are mainly located on the boundaries of high/low velocity regions (Figs 6, 7 and 12), with a characteristic  
365 depth between 5 and 15 km. The distribution of well located hypocenters reveals a number of patterns related to

366 structures inferred from other evidences. Among others we note foci accompanying the Armo – Delianuova as well as  
367 the Reggio Calabria fault lineaments. Other event locations are found along alignments parallel to the eastern coast of  
368 Sicily. High precision relocation of the multiplet family S2 revealed a similar trend, furnishing further evidence for the  
369 presence of a NNE striking element. In the southern part of the investigated area, there is an increase of focal depth up  
370 to 40 km for the events south of the Calabrian coast (Fig. 9). Here, a rather irregular distribution of hypocenters makes  
371 it difficult to identify underlying tectonic structures. On the other hand, the mapping of geological structures is hindered  
372 by the sea cover, reaching depths of over 1000 m in the studied area.

373 Concerning fault plane solutions, earthquakes located in the Messina Strait, the Peloritani Mountains (Scarfì et al.,  
374 2005) and adjacent areas on the Calabrian land side reveal a normal faulting mechanism along NNE or NE striking  
375 planes, which is consistent with the overall regional trends of tectonic motion, i. e. extension in WNW-ESE direction.  
376 Strike slip mechanism was found for two events located offshore Cape Taormina, but again with P-axis striking NNE.  
377 The focal mechanisms of earthquakes falling in the Ionian Sea, south of the Calabrian coast, reveal a change of the  
378 stress field as P-axes striking in NW direction prevail.

379 In conclusion, the various seismological features – 3D velocity structure, seismicity patterns, fault plane solutions -  
380 confirm that important tectonic elements visible at the surface reach a considerable depth, at least down to the levels  
381 illuminated by earthquake activity. The graben-like structure is well identifiable in the calabrian inland and continues  
382 underneath the Messina Strait. The northeastern coastline of Sicily from Taormina to Messina is accompanied by  
383 considerable velocity contrasts well identifiable down to a depth of 12 to 15 km. The Messina Strait as well as the  
384 adjacent Peloritani Mountains are characterized by extension perpendicular to the NNE striking elements. Both  
385 hypocenter locations and focal mechanisms suggest that seismotectonic characteristics in the southern part differ from  
386 the picture found in the Messina Strait and adjacent zones. In particular, focal depths of the events increase and the  
387 principal direction of major horizontal stress turns from NNE to NW.

388

### 389 **Acknowledgments**

390 We wish to thank H. Zhang for allowing us to use the code TomoADD, our colleagues P. De Gori and A. Amato at  
391 INGV-CNT for providing data from National seismic network and two anonymous reviewers for carefully reading the  
392 manuscript and their constructive criticism. Helpful suggestions by the editor, George Helffrich, are also highly  
393 appreciated.

394

395 **References**

- 396 Anderson, H., and Jackson, J., 1987. The deep seismicity of the Tyrrhenian Sea. *Geophys. J. R. Astr. Soc.* 91, 613-637.
- 397 Barberi, F., Gasparini, P., Innocenti, F., Villari, L., 1973. Volcanism of the Southern Tyrrhenian Sea and its  
398 geodynamic implications. *J. Geophys. Res.* 78, 5221-5232.
- 399 Barberi, G., Cosentino, M.T., Gervasi, A., Guerra, I., Neri, G., Orecchio, B., 2004. Crustal seismic tomography in the  
400 Calabrian Arcregion, south Italy. *Phys. Earth Planet. Inter.* 147, 297-314.
- 401 Boschi, E., Guidoboni, E., Ferrari, G., Mariotti, D., Valensise, G., 2000. Catalogue of strong Italian earthquakes, *Ann.*  
402 *Geofis.* 43, 268.
- 403 Bottari, A., Carapezza, E., Carapezza, M., Carveni, P., Cefali, F., Lo Giudice, E., Pandolfo, C., 1986. The 1908 Messina  
404 Strait earthquake in the regional geosstructural frame work. *J. Geodyn.*, 5, 275-302.
- 405 CFTI-Med 4.0, Guidoboni, E., Ferrari, G., Mariotti, D., Comastri, A., Tarabusi, G., Valensise, G. Catalogue of strong  
406 earthquakes in Italy 461 B.C. – 1997 and Mediterranean area 760 B.C. – 1500. An advanced Laboratory of  
407 historical seismology, <http://storing.ingv.it/cfti4med/>.
- 408 CPTI Work Group, 2004. Catalogo Parametrico dei Terremoti Italiani, versione 2004 (CPTI04). INGV, Bologna,  
409 <http://emidius.mi.ingv.it/CPTI04/>.
- 410 DISS Working Group, 2005. Database of Individual Seismogenic Sources (DISS), Version 3.0.1: a compilation of  
411 potential sources for earthquakes larger than M 5.5 in Italy and surrounding areas. INGV, Roma,  
412 <http://diss.rm.ingv.it/diss/>
- 413 D'Agostino, N., and Selvaggi, G., 2004. Crustal motion along the Eurasia-Nubia plate boundary in the Calabrian Arc  
414 and Sicily and active extension in the Messina Straits from GPS measurements. *J. Geophys. Res.* 109, B11402,  
415 doi:10.1029/2004JB002998.
- 416 Evans, J.R., Eberhart-Phillips, D., Thurber, C.H., 1994. User's manual for simulps12 for imaging Vp and Vp/Vs: a  
417 derivative of the "Thurber" tomographic inversion simul3 for local earthquakes and explosions. USGS Open-file  
418 Report, pp. 94–431.
- 419 Finetti, I., and Del Ben, A., 1986. Geophysical study of the Tyrrhenian opening. *Boll. Geof. Teor. Appl.* 110, 75-155.
- 420 Galli, P., 2000. New empirical relationships between magnitude and distance for liquefaction, *Tectonophysics* 324, 169-  
421 187.
- 422 Gasparini, C., Iannaccone, G., Scandone, P., Scarpa, R., 1982. Seismotectonics of the Calabrian Arc. *Tectonophysics*  
423 84, 267-286.
- 424 Ghisetti, F., 1984. Recent deformations and the seismogenic source in the Messina Strait (Southern Italy).  
425 *Tectonophysics* 210, 117-133.



- 426 Ghisetti, F., 1992. Fault parameters in the Messina Strait (southern Italy) and relations with the seismogenic source.  
427 *Tectonophysics* 210, 117-133.
- 428 Giammanco, S., Palano M., Scaltrito A., Scarfi L., Sortino F., 2008. Possible role of fluid 461 overpressure in the  
429 generation of earthquake swarms in active tectonic areas: The case of 462 the Peloritani Mts. (Sicily, Italy). *J. Volc.*  
430 *Geoth. Res.*, 178, 795-806, doi: 463 10.1016/j.jvolgeores.2008.09.005.
- 431 Giardini, D., and Velonà, M., 1991. The deep seismicity of the Tyrrhenian Sea. *Terra Nova* 3, 57-64.
- 432 Haslinger, F., Kissling, E., Ansorge, J., Hatzfeld, D., Papadimitriou, E., Karakostas, V., Makropoulos, K., Kahle, H.G.,  
433 Peter, Y., 1999. 3-D crustal structure from local earthquake tomography around the Gulf of Arta (Ionian region,  
434 NWGreece). *Tectonophysics* 304, 201–218.
- 435 Husen, S., Kissling, E., Flueh, E., Asch, G., 1999. Accurate hypocentre determination in the seismogenic zone of the  
436 subducting Nazca plate in northern Chile using a combined on-/offshore network. *Geophys. J. Int.* 138: 687-701.
- 437 Langer, H., Raffaele, R., Scaltrito, A., Scarfi, L., 2007. Estimation of an optimum Velocity Model in the Peloritani  
438 Mountains – Assessment of the variance of model parameters and variability of earthquake locations. *Geophys. J.*  
439 *Int.* 170, 3, 1151-1164, doi: 10.1111/j.1365-246X.2007.03459.x.
- 440 Lentini, F., Catalano, S. & Carbone, S., 2000. Carta geologica della provincia di Messina, Provincia Regionale di  
441 Messina. Assessorato Territorio–Servizio geologico, SELCA, Firenze.
- 442 Menke, W., and Schaff, D., 2004. Absolute earthquake locations with differential data. *Bull. Seism. Soc. Am.* 94, 2254  
443 –2264.
- 444 Monaco, C., and Tortorici, L., 2000. Active faulting in the Calabrian Arc and eastern Sicily. *Journal of Geodynamics*  
445 29, 407-424.
- 446 Murphy, W., 1995. The geomorphological controls on seismically triggered landslides during the 1908 Straits of  
447 Messina earthquake, Southern Italy. *Quarterly Journal of Engineering Geology and Hydrogeology* 28, 61-74, doi:  
448 10.1144/GSL.QJEGH.1995.028.P1.06.
- 449 Neri, G., Barberi, G., Oliva, G., Orecchio, B., 2004. Tectonic stress and seismogenic faulting in the area of the 1908  
450 Messina earthquake, south Italy. *Geophys. Res. Lett.* 31, 10, doi:10.1029/2004GL019742.
- 451 Patacca, E., Sartori, R., and Scandone, P., 1990. Tyrrhenian basin and Appenninic arcs: kinematic relations since late  
452 Tortonian times. *Mem. Soc. Geol. It.*, 45, 425-451.
- 453 Raffaele, R., Langer, H., Gresta, S., Moia, F., 2006. Tomographic inversion of local earthquake data from the Gioia  
454 Tauro basin (south-western Calabria, Italy). *Geophys. J. Int.* 165, doi: 10.1111/j.1365-246X.2006.02872.x

- 455 Reasenber, P. A., and Oppenheimer, D., 1985. FPFIT, FPLOT and FPPAGE: fortran computer programs for  
456 calculating and displaying earthquake fault-plane solutions. Open File Rep., 85-379, 109 pp., U. S. Geol. Surv.,  
457 Washington.
- 458 Scarfi, L., Langer, H., Gresta, S., 2003. High-precision relative locations of two microearthquake clusters in  
459 southeastern Sicily, Italy. *Bull. seism. Soc. Am.* 93, 1479–1497.
- 460 Scarfi, L., Langer, H., Scaltrito, A., 2005. Relocation of microearthquake swarms in the Peloritani mountains –  
461 implications on the interpretation of seismotectonic patterns in NE Sicily, Italy. *Geophys. J. Int.* 163, 225-237, doi:  
462 10.1111/j.1365-246X.2005.02720.x.
- 463 Scarfi, L., Giampiccolo, E., Musumeci, C., Patanè, D., Zhang, H., 2007. New insights on 3D crustal structure in  
464 southeastern Sicily (Italy) and tectonic implications from an adaptive mesh seismic tomography. *Phys. Earth  
465 Planet. Int.* 161, 74-85.
- 466 Selvaggi, G., and Chiarrabba, C., 1995. Seismicity and P-wave velocity image of the Southern Tyrrhenian subduction  
467 zone, *Geophys. J. Int.* 121, 818-826.
- 468 Stüwe, K., 2002. *Geodynamics of the Lithosphere*, Springer-Verlag Berlin Heidelberg, pp. 449.
- 469 Tertulliani, A., Cucci L., 2008. Fenomeni associati al terremoto della Calabria dell'8 settembre 1905. *Quaderni di  
470 Geofisica.*, 60.
- 471 Tortorici, L., Monaco, C., Tansi, C., Cocina, O., 1995. Recent and active tectonics in the Calabrian Arc (southern Italy).  
472 *Tectonophysics*, 243, 37–55.
- 473 Um, J., and Thurber, C.H., 1987. A fast algorithm for two-point seismic ray tracing. *Bull. Seismol. Soc. Am.* 77, 972-  
474 986.
- 475 Valensise, G., and Pantosti, D., 1992. A 125 kyr-long geological record of seismic source repeatability: the Messina  
476 Straits (southern Italy) and the 1908 earthquake (Ms 7.1/2). *Terra Nova*, 4, 472-483.
- 477 Waldhauser, F., and Ellsworth, W. L., 2000. A double-difference earthquake location algorithm: Method and  
478 application to North Hayward Fault, California. *Bull. Seism. Soc. Am.*, 90, 1353-1368.
- 479 Zhang, H., Thurber, C.H., 2003. Double-difference tomography: The method and its application to the Hayward fault,  
480 California. *Bull. Seismol. Soc. Am.* 93, 1875-1889.
- 481 Zhang, H., Thurber, C.H., 2005. Adaptive mesh seismic tomography based on tetrahedral and Voronoi diagrams:  
482 Application to Parkfield, California. *J. Geophys. Res.* 110, B04303, doi:10.1029/2004JB003186.
- 483 Zhao, D., Hasegawa, A., Horiuchi, S., 1992. Tomographic imaging of P and S wave velocity structure beneath  
484 northeastern Japan. *J. Geophys. Res.* 97, 19909-19928.

485

486

487 **Figure Captions**

488

489 Fig. 1. Simplified tectonic map (a) and structural sketch map (b) of Sicily and southern Calabria (from Ghisetti, 1992;  
490 Lentini et al., 2000). ATG is the abbreviation for Aeolian-Tindari-Giardini faults lineament. Permanent seismic network  
491 is also reported: black triangles for Mt. Etna and Aeolian Islands networks and black/white boxes for northeastern Sicily  
492 and southern Calabria. Dashed boxes represent the area studied in this paper.

493

494 Fig. 2. Map view, N-S and E-W cross sections of the studied area with earthquakes located from 1999 to 2007.

495

496 Fig. 3. 3D sketch of P-wave ray paths traced in the minimum 1D model (Langer et al., 2007). Earthquakes and seismic  
497 stations are indicated by red circles and blue triangles, respectively.

498

499 Fig. 4. Irregular mesh nodes (triangles) for P- (a) and S-waves (b) at the final iteration. At the bottom of the sketches,  
500 the projection of the mesh (crosses) and the map of the area (black contour line) are shown.

501

502 Fig. 5. DWS value distribution for P waves for the regular inversion grid (a) and irregular inversion mesh (b) at the final  
503 iteration (zero values are not shown).

504

505 Fig. 6. a) Map of the studied area with the main structural features (from Ghisetti, 1992; Lentini et al., 2000); b) P-wave  
506 velocity model for six representative layers resulting from the 3D inversion. Contour lines are at 0.2 km/s intervals. Red  
507 circles represent the relocated earthquakes within half the grid size of the slice. The zones with  $DWS > 100$  are  
508 circumscribed by yellow contour lines.

509

510 Fig. 7. Vertical sections through the P-wave velocity model. The traces of sections are reported in the sketch map (A-  
511 A", ... F-F"). Contour lines are at 0.4 km/s intervals. White curves contour the zones with  $DWS > 100$ . Relocated  
512 earthquakes, within  $\pm 4$  km from the sections, are plotted as red circles.

513

514 Fig. 8. P-wave velocity distribution obtained from the characteristic (a) and restoring (b) resolution tests (see text for  
515 further details).

516

517 Fig. 9. Final event locations in map and vertical sections. The main fault systems are also shown in the map.

518

519 Fig. 10. Relative locations of S1 and S2 clusters by using the master-event-technique. Map view (a), vertical cross-  
520 sections (b, c) and 3 D sketch (d).

521

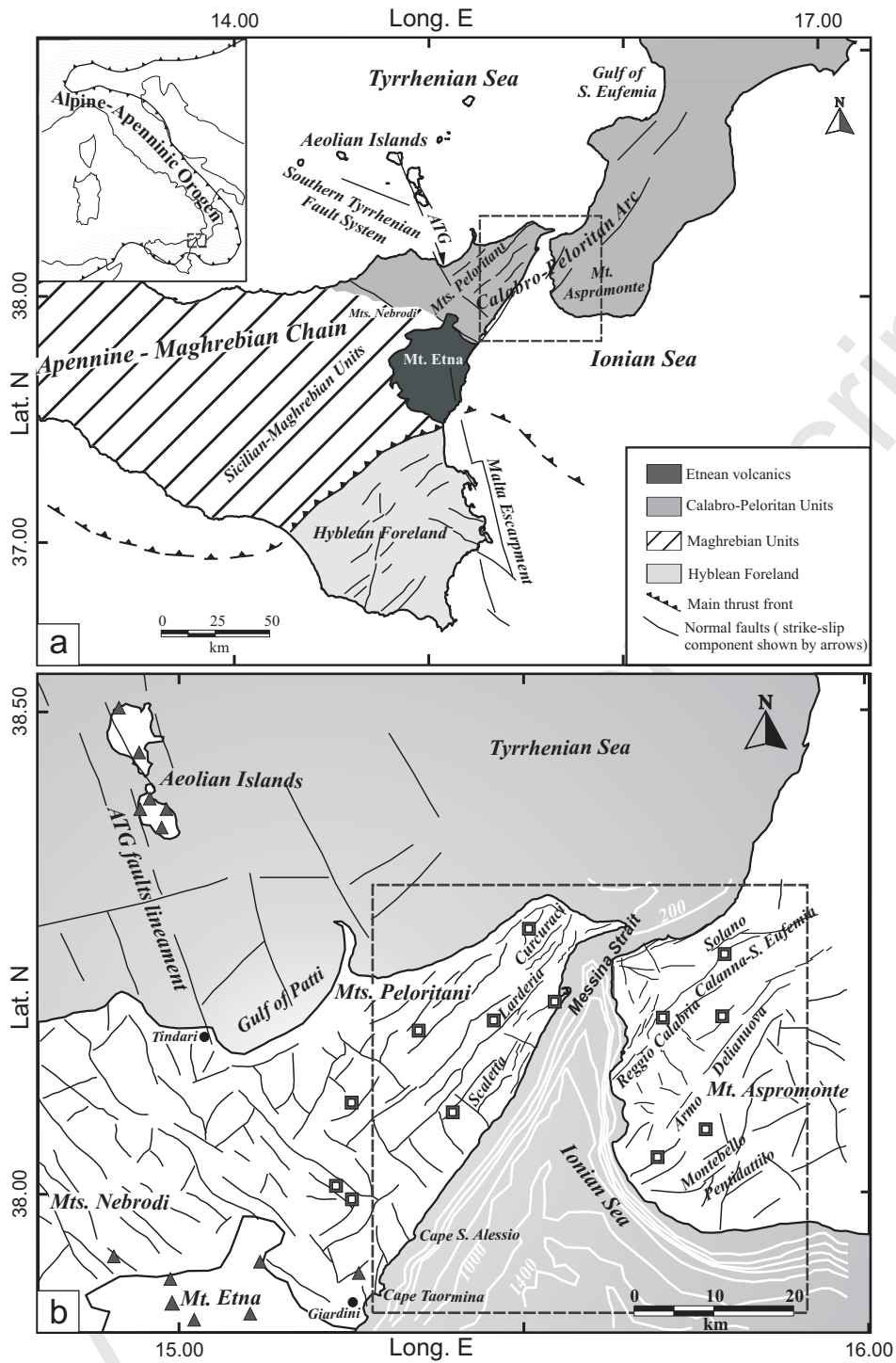
522 Fig. 11. Focal mechanisms of the major events of the northeastern Sicily and southern Calabria. Their depth are  
523 represented together with the fault plane solutions, e. g.  $Z = 11$  (km).

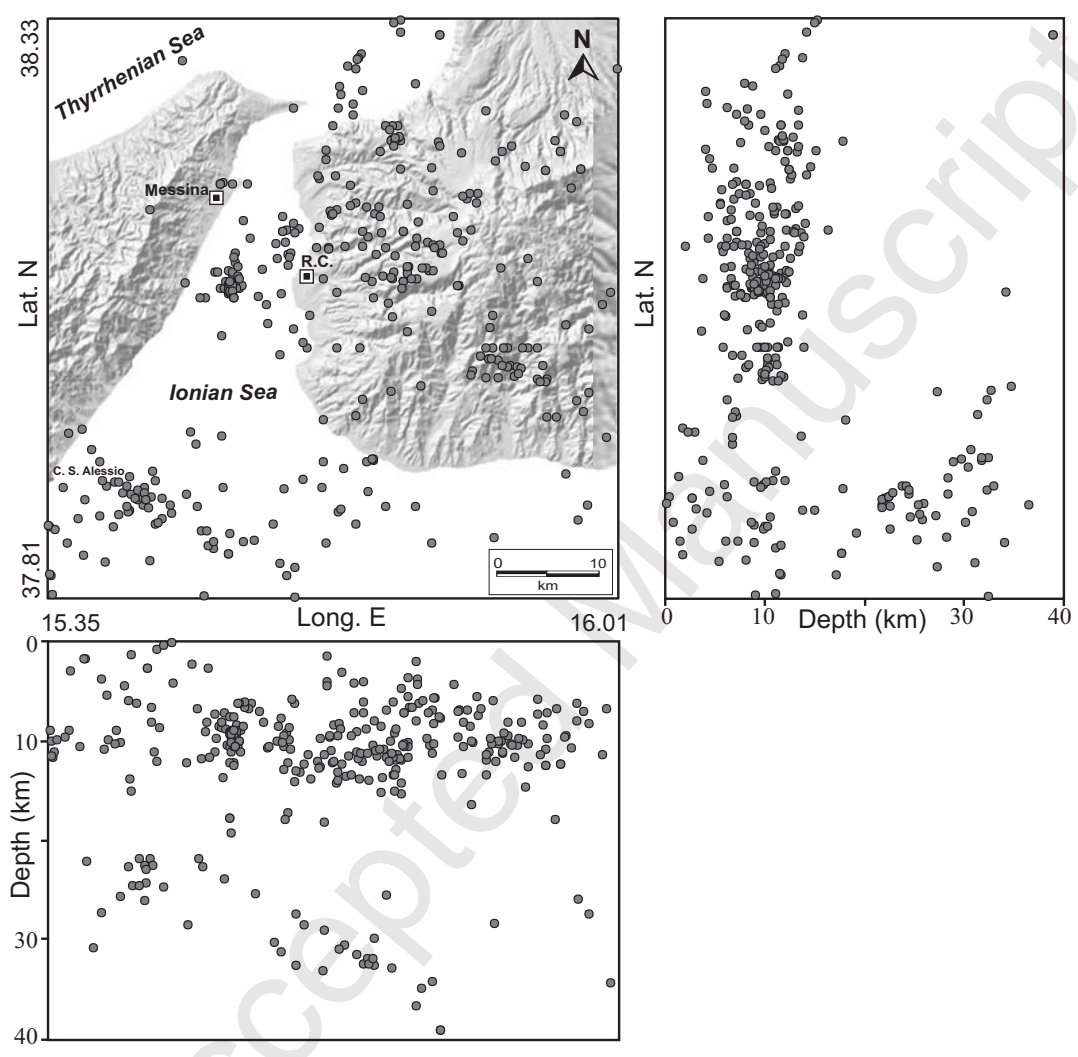
524

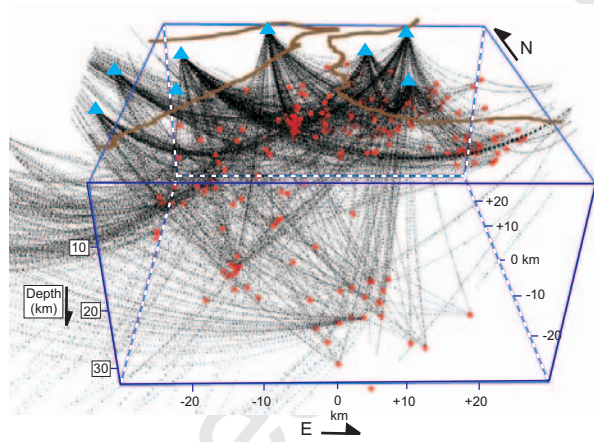
525 Fig. 12. Topography of the 6.5 km/s P-wave velocity isosurface. Darker colours indicate a greater depth. Contours are at  
526 2.5 km intervals and the numbers indicate the corresponding depths. Relocated earthquakes, above the isosurface, are  
527 plotted as red circles.

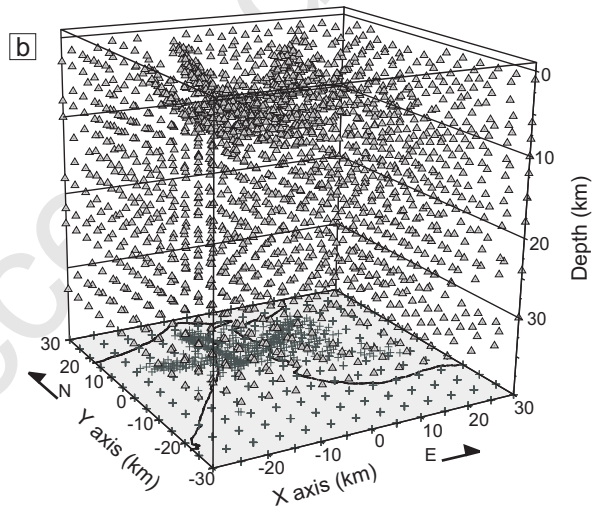
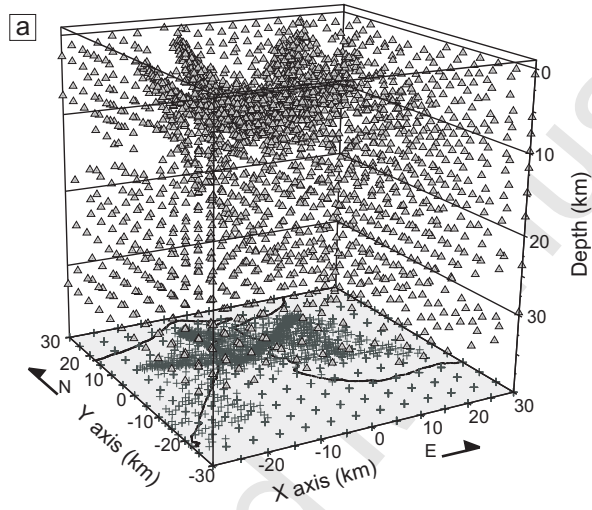
528

Accepted Manuscript











Manuscript

